RIS-Enabled Self-Localization: Leveraging Controllable Reflections With Zero Access Points

Kamran Keykhosravi*, Gonzalo Seco-Granados†, George C. Alexandropoulos‡, and Henk Wymeersch*

* Department of Electrical Engineering, Chalmers University of Technology, Sweden
† Department of Telecommunications and Systems Engineering, Universitat Autonòma de Barcelona, Spain
‡Department of Informatics and Telecommunications, National and Kapodistrian University of Athens, Greece
emails: {kamrank, henkw}@chalmers.se, gonzalo.seco@uab.es, alexandg@di.uoa.gr

Abstract—Reconfigurable intelligent surfaces (RISs) are one of the most promising technological enablers of the next (6th) generation of wireless systems. In this paper, we introduce a novel use-case of the RIS technology in radio localization, which is enabling the user to estimate its own position via transmitting orthogonal frequency-division multiplexing (OFDM) pilots and processing the signal reflected from the RIS. We demonstrate that user localization in this scenario is possible by deriving Cramér-Rao lower bounds on the positioning error and devising a low-complexity position estimation algorithm. We consider random and directional RIS phase profiles and apply a specific temporal coding to them, such that the reflected signal from the RIS can be separated from the uncontrolled multipath. Finally, we assess the performance of our position estimator for an example system, and show that the proposed algorithm can attain the derived bound at high signal-to-noise ratio values.

Index Terms—Radio localization, reconfigurable intelligent surface, maximum likelihood estimation, radar.

I. INTRODUCTION

Reconfigurable intelligent surfaces (RISs) are expected to revolutionize wireless systems by enabling smart radio environments, where the propagation channel can also be programmed to improve the Quality of Service (QoS) [1], [2]. In general, an RIS can be modeled as a planar array of sub-wavelength unit cells, each of which can scatter the impinging signal after modulating its phase in a controlled fashion [3]. The RIS phase profile can then be designed for optimal beam-forming, localization, or interference management. Recently, a large body of research has been devoted to study the modeling, control, phase-profile design, and potential use-cases of RISs for both communications and radio localization [4]. With radio localization (which is the main topic of this paper) RISs can enable or boost the accuracy of user equipment (UE) positioning by providing: *i)* a strong reflected signal path towards the UE, and *ii)* a reference position [5]. Being cost- and energy-efficient, RISs have the potential to boost/enable radio localization in a wide variety of situations, specifically in those where GPS signal is unavailable or weak, e.g., in city canyons, indoor environments, and tunnels.

Many studies have been conducted to investigate RIS-aided localization in different scenarios, which can be categorized in terms of the operating regime (near-field [6]–[9], far-field [10]–[12]), RIS placement (at the base station (BS) side [7],
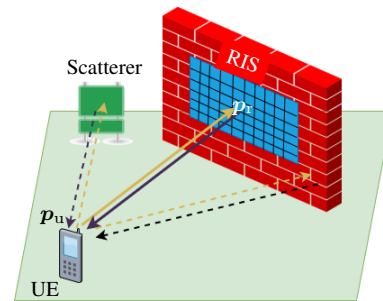

Fig. 1. The considered system setup with a single-antenna UE and an RIS. The wireless environment is assumed to also include passive objects contributing to multipath signal reflection.

[8], at the UE side [12], or as a separate reflector [13], [14]), wireless settings (multiple-input multiple-output (MIMO) [14], [15], multiple-input single-output (MISO) [10], and single-input single-output (SISO) [9], [11]), etc. Furthermore, RISs can be used to assist the radar systems to improve the target detection capabilities [16], [17]. In [7], Cramér-Rao lower bounds (CRB) on the localization error were established for the near-field of a continuous RIS and the effects of the RIS size were studied. For the same scenario, the effects of limited RIS phase resolution was investigated in [18]. In [8], localization with an RIS acting as a lens has been considered and an estimation algorithm was proposed. Near-field localization with one BS and an RIS has been studied in [6], [9], where it is shown that the wavefront curvature can be used to localize the UE, even if the direct path from the BS to UE is blocked. Specifically, the authors in [6] illustrated that by using a large stripe-like RIS, positioning can be performed even if the RIS is severely obstructed. For a generic MIMO setting equipped with an RIS, the CRBs have been developed on location and orientation errors in [14]. In [15], the authors considered an RIS-aided MIMO scenario, derived the CRBs, and used the bounds to optimize the RIS phase profile for localization. Furthermore, it has been shown that localization and UE synchronization can be performed in a MISO [10] and even in a SISO [11] setup with the help of a single RIS, when far-field conditions hold.

In this paper, we present a novel use-case for RIS-enabled

localization, where an RIS is used to reflect the signal transmitted from the UE back to the UE itself, and there are no access points or BSs present (see Fig. 1). We establish the channel model for orthogonal frequency-division multiplexing (OFDM) transmission by taking into account the undesired multipath from the surrounding environment. This multipath is then removed via a specific RIS profile design and a postprocessing step at the UE side. Next, we estimate the user position by first obtaining a coarse estimate and then refining it to maximize the likelihood function. Finally, we evaluate our estimation method and compare its accuracy to our derived CRBs. It is shown that the proposed estimator attains the bounds at high signal-to-noise ratios (SNRs).

Notations: Vectors are shown by bold lower-case letters and matrices by bold upper-case ones. We use $[\boldsymbol{a}]_i$ to indicate the ith element of the vector $\boldsymbol{a}$ and $[\boldsymbol{A}]_{i,j}$ to denote the element at the ith row and the jth column of matrix $\boldsymbol{A}$. Furthermore, the subindex $i : j$ is used to specify all the elements between i and j. All vectors are column vectors by default. Transpose, Hermitian, and complex-conjugate operations are denoted by $(\cdot)^\top$, $(\cdot)^{\mathrm{H}}$, and $(\cdot)^*$, respectively. The Hadamard product is indicated by $\odot$.

II. SYSTEM AND CHANNEL MODEL

We consider a single-antenna full-duplex UE with unknown location $\boldsymbol{p}_{\mathrm{u}} \in \mathbb{R}^3$ and a single RIS with known center location $\boldsymbol{p}_{\mathrm{r}} \in \mathbb{R}^3$ and orientation $\boldsymbol{R} \in \mathrm{SO}(3)$. We assume that the RIS is handled by a dedicated controller with whom the UE can communicate for establishing synchronization [4]. The UE location relative to the RIS is defined as $\boldsymbol{p}_{\mathrm{ur}} = \boldsymbol{p}_{\mathrm{u}} - \boldsymbol{p}_{\mathrm{r}}$. The RIS has M elements in a square configuration. We indicate the location of the mth RIS element by $\boldsymbol{p}_{\mathrm{r},m}$. The UE transmits T OFDM signals with N subcarriers and receives the backscattered signals from the RIS and from some other scatterers in the environment. We assume that the UE-RIS (or RIS-UE) channel has negligible non line-of-sight (NLOS) components. Furthermore, we assume that all the transmitted pilot symbols are equal to $\sqrt{E_{\mathrm{s}}}$, with E_{s} being the symbol energy. Then, the received signal at the UE at the discrete time $t = 1, 2, \ldots, T$ can be modeled as follows:

$$\boldsymbol{y}_t \triangleq \sqrt{E_{\mathrm{s}}}\beta_0 \boldsymbol{d}(\tau_0)\boldsymbol{a}(\boldsymbol{p}_{\mathrm{ur}})^\top \boldsymbol{\Omega}_t \boldsymbol{a}(\boldsymbol{p}_{\mathrm{ur}})$$
$$+ \sqrt{E_{\mathrm{s}}}\sum_{l=1}^{L}\beta_l \boldsymbol{d}(\tau_l) + \boldsymbol{n}_t. \quad (1)$$

Here, $\tau_0 \triangleq 2\|\boldsymbol{p}_{\mathrm{ur}}\|/c$ is the transmission delay, where c is the speed of light. The delay steering vector is defined as

$$\boldsymbol{d}(\tau) \triangleq [1, e^{-\jmath 2\pi\tau\Delta f}, \ldots, e^{-\jmath 2\pi\tau(N-1)\Delta f}]^\top, \quad (2)$$

where Δf is the subcarrier spacing. The complex channel gain is denoted by $\beta_0 \in \mathbb{C}$. The vector $\boldsymbol{a}(\boldsymbol{p}_{\mathrm{ur}}) \in \mathbb{C}^M$ indicates the RIS response, having the elements for $m = 1, 2, \ldots, M$:

$$[\boldsymbol{a}(\boldsymbol{p}_{\mathrm{ur}})]_m = \exp\left(\jmath\frac{2\pi}{\lambda}(\|\boldsymbol{p}_{\mathrm{u}} - \boldsymbol{p}_r\| - \|\boldsymbol{p}_{\mathrm{u}} - \boldsymbol{p}_{\mathrm{r},m}\|)\right), \quad (3)$$

where $\lambda \triangleq c/f_{\mathrm{c}}$ is the wavelength with f_{c} being the carrier frequency. Furthermore, we have $\boldsymbol{\Omega}_t \triangleq \mathrm{diag}(\boldsymbol{\omega}_t)$, where $\boldsymbol{\omega}_t \in \mathbb{C}^M$ is the RIS phase profile, i.e., for each m, the amplitude of $[\boldsymbol{\omega}_t]_m$ is one and its phase indicates the phase shift applied by the mth element of RIS to the impinging signal. The noise term $\boldsymbol{n}_t$ is assumed to be spatially and temporally white with covariance $\sigma_{\mathrm{n}}^2 \boldsymbol{I}_N$. The number of uncontrolled multipath components is denoted by L. The path loss and the delay for the ℓth path are denoted by β_ℓ and τ_ℓ, respectively. By using the following definition:

$$\boldsymbol{b}(\boldsymbol{p}_{\mathrm{ur}}) \triangleq \boldsymbol{a}(\boldsymbol{p}_{\mathrm{ur}}) \odot \boldsymbol{a}(\boldsymbol{p}_{\mathrm{ur}}), \quad (4)$$

we can rewrite (1) in the more compact form:

$$\boldsymbol{y}_t = \sqrt{E_{\mathrm{s}}}\beta_0 \boldsymbol{d}(\tau_0)\boldsymbol{b}(\boldsymbol{p}_{\mathrm{ur}})^\top \boldsymbol{\omega}_t + \sqrt{E_{\mathrm{s}}}\sum_{l=1}^{L}\beta_l \boldsymbol{d}(\tau_l) + \boldsymbol{n}_t. \quad (5)$$

We assume that the UE has the knowledge of the RIS location and orientation and also the RIS phase profiles $\boldsymbol{\Omega}_t$, which change over time; this information can be communicated by the RIS controller. This controller also coordinates the start of the pilot transmission with the UE. Using these system control settings, the UE's goal is to estimate its position via its received signal $\boldsymbol{y}_t$. We next establish the requirement for the RIS element spacing in order to avoid ambiguities in the UE position estimation.

Remark 1. *To avoid grating lobes, which causes ambiguity in the position estimation at the far field, the RIS element spacing should be at least $\lambda/4$. To show this, we rewrite the far-field approximation of the vector $\boldsymbol{b}(\boldsymbol{p}_{\mathrm{u}})$ in (4) for a two-dimensional (2D) case with an $1 \times M$ uniform linear array (ULA) RIS, as $[\boldsymbol{b}_{\mathrm{ff}}(\theta)]_m = \exp(\jmath\frac{4\pi}{\lambda}md\sin\theta)$, where θ is the angle between $\boldsymbol{p}_{\mathrm{ur}}$ and the RIS normal. Since we assume that the UE is placed in the front side of the RIS, we have that $\theta = [-\pi/2, \pi/2]$, and hence, $\sin(\theta) = [-1, 1]$. Therefore, the phase difference between two consecutive entries of the vector $\boldsymbol{b}_{\mathrm{ff}}(\theta)$ is between $[-\jmath 4\pi d/\lambda \ \jmath 4\pi d/\lambda]$. Consequently, it must hold $8\pi d/\lambda \leq 2\pi$, resulting in $d \leq \lambda/4$, to be able to find θ without ambiguity.*

III. RIS PHASE PROFILE DESIGN

In this section, we study the design of the RIS phase profile $\boldsymbol{\omega}_t$. First, we describe how to design $\boldsymbol{\omega}_t$ to remove the uncontrolled multipath at the UE's receiver, and then, we introduce the random and directional RIS phase profiles, which are used in simulation results in Section VI.

A. Multipath Removal

To remove the multipath from the received signal in (5), using the method presented in [19]. First, we design the RIS phase profiles for half of the transmission time and denote them by $\tilde{\boldsymbol{\omega}}_{\tilde{t}} \in \mathbb{C}^M$, where $\tilde{t} = 1, 2, \ldots, T/2$ (T is assumed even). The vectors $\tilde{\boldsymbol{\omega}}_{\tilde{t}}$ can be chosen based on a random codebook (explained later on in Section III-B), a directional one (explained in Section III-C), or any other strategy. Then,

we let $\boldsymbol{\omega}_{2\tilde{t}-1} = \tilde{\boldsymbol{\omega}}_{\tilde{t}}$ and $\boldsymbol{\omega}_{2\tilde{t}} = -\tilde{\boldsymbol{\omega}}_{\tilde{t}}$. Consequently, at the UE receiver, we compute the following quantity:

$$\tilde{\boldsymbol{y}}_{\tilde{t}} = \frac{1}{2}(\boldsymbol{y}_{2\tilde{t}-1} - \boldsymbol{y}_{2\tilde{t}}) \tag{6}$$

$$= \sqrt{E_{\mathrm{s}}}\beta_0 \boldsymbol{d}(\tau_0) \boldsymbol{b}(\boldsymbol{p}_{\mathrm{ur}})^\top \tilde{\boldsymbol{\omega}}_{\tilde{t}} + \tilde{\boldsymbol{n}}_t, \tag{7}$$

where (7) follows from (5) and $\tilde{\boldsymbol{n}}_t$ is a white complex Gaussian noise with covariance matrix $\sigma_{\mathrm{n}}^2/2\boldsymbol{I}_N$. It can be seen that the multipath contribution has been disappeared in (7).

B. Random Codebook

The random codebook is used when there exists no prior knowledge of the UE location. With this codebook, we have $[\tilde{\boldsymbol{\omega}}_t]_m = \exp(\jmath\theta_{m,t})$, where $\theta_{m,t}$ $\forall m,t$ are chosen randomly according to the uniform distribution over the interval $[0, 2\pi)$, each one independently from each other.

C. Directional Codebook

We use the directional codebook when there exists a prior knowledge about the UE position. We assume that an approximate location $\boldsymbol{q}_{\mathrm{u}}$ is available, which is distributed uniformly within the sphere $\mathcal{S}(\boldsymbol{p}_{\mathrm{u}}, \delta)$, with δ being the uncertainty radius, and for any $\boldsymbol{c} \in \mathbb{R}^3$ and $r \in \mathbb{R}^+$ holds:

$$\mathcal{S}(\boldsymbol{c}, r) = \{\boldsymbol{x} \in \mathbb{R}^3 \big| \|\boldsymbol{c} - \boldsymbol{x}\| \le r\}. \tag{8}$$

To generate a directional codebook, we first select $T/2$ points $\boldsymbol{q}_{\mathrm{u},\tilde{t}} \in \mathbb{R}^3$, with $\tilde{t} = 1, 2, \ldots, T/2$, randomly and uniformly within the sphere $\mathcal{S}(\boldsymbol{q}_{\mathrm{u}}, \delta)$. Then, we design the RIS phase profiles as:

$$\tilde{\boldsymbol{\omega}}_{\tilde{t}} = \boldsymbol{b}(\boldsymbol{q}_{\mathrm{u},\tilde{t}} - \boldsymbol{p}_{\mathrm{r}})^*. \tag{9}$$

It can be seen that by assigning the RIS phase profile according to the latter expression, the reflected signal power is directed towards the points $\boldsymbol{q}_{\mathrm{u},\tilde{t}}$.

IV. FISHER INFORMATION ANALYSIS

In this section, we present an analytical lower bound on the estimation error based on the Fisher information matrix (FIM) analysis. For all unbiased estimators, the estimation error is lower-bounded by the position error bound (PEB), that is

$$\mathrm{PEB} \triangleq \sqrt{\mathrm{tr}\left([\boldsymbol{J}(\boldsymbol{\eta})^{-1}]_{3:5,3:5}\right)}. \tag{10}$$

Here, $\boldsymbol{\eta} \in \mathbb{R}^{5+3L}$ is the vector of unknowns that is

$$\boldsymbol{\eta} \triangleq [\rho_0, \varphi_0, \boldsymbol{p}_{\mathrm{u}}^\top, \rho_1, \varphi_1, \tau_1, \ldots, \rho_L, \varphi_L, \tau_L]^\top, \tag{11}$$

where $\rho_l = |\beta_l|$ and $\varphi_l = \angle\beta_l$ for $l = 0, 1, \ldots, L$. Furthermore, $\boldsymbol{J}(\boldsymbol{\eta})$ is the FIM, which is defined as [20]

$$\boldsymbol{J}(\boldsymbol{\eta}) \triangleq \frac{2E_{\mathrm{s}}}{\sigma_{\mathrm{n}}^2} \Re\left\{\sum_{t=1}^T \left(\frac{\partial\boldsymbol{\mu}_t}{\partial\boldsymbol{\eta}}\right)^{\mathrm{H}} \frac{\partial\boldsymbol{\mu}_t}{\partial\boldsymbol{\eta}}\right\}, \tag{12}$$

where $\boldsymbol{\mu}_t \triangleq \beta_0 \boldsymbol{d}(\tau_0)\boldsymbol{b}(\boldsymbol{p}_{\mathrm{ur}})^\top\boldsymbol{\omega}_t + \sum_{l=1}^L \beta_l \boldsymbol{d}(\tau_l)$. Next, we study the structure of the FIM when the temporal sum of the utilized RIS phase profiles (i.e., $\sum_t \boldsymbol{\omega}_t$) becomes the all-zero

vector. This includes (but is not restricted to) the codebooks discussed in Section III.

Proposition 1. *In the FIM expression given by (12), any element of the form:*

$$\sum_{t=1}^T \left(\frac{\partial\boldsymbol{\mu}_t}{\partial\eta_{LOS}}\right)^H \frac{\partial\boldsymbol{\mu}_t}{\partial\eta_{NLOS}} \tag{13}$$

for any $\eta_{LOS} \in \boldsymbol{\eta}_{LOS} \triangleq [\rho_0, \varphi_0, \boldsymbol{p}_{\mathrm{u}}^\top]^\top$ *and any* $\eta_{NLOS} \in [\rho_1, \varphi_1, \tau_1, \ldots, \rho_L, \varphi_L, \tau_L]^\top$ *evaluates to zero, provided that* $\sum_t \boldsymbol{\omega}_t = \boldsymbol{0}$ *holds.*

Proof. Any term of the form $\partial\boldsymbol{\mu}_t/\partial\eta_{LOS}$ depends linearly on $\boldsymbol{\omega}_t$, while any term $\partial\boldsymbol{\mu}_t/\partial\eta_{NLOS}$ is independent of $\boldsymbol{\omega}_t$. Since $\sum_t \boldsymbol{\omega}_t = \boldsymbol{0}$, the corresponding entry in the FIM will evaluate to zero. $\square$

Based on Proposition 1, the FIM has the following structure:

$$\boldsymbol{J}(\boldsymbol{\eta}) = \begin{bmatrix} \boldsymbol{J}(\boldsymbol{\eta}_{\mathrm{LOS}}) & \boldsymbol{0} \\ \boldsymbol{0} & \boldsymbol{J}(\boldsymbol{\eta}_{\mathrm{NLOS}}) \end{bmatrix}, \tag{14}$$

where $\boldsymbol{0}$ indicates the all-zero matrix and $\boldsymbol{J}(\boldsymbol{\eta}_{\mathrm{LOS}})$ and $\boldsymbol{J}(\boldsymbol{\eta}_{\mathrm{NLOS}})$ are defined similar to (12). Using the Schur's complement method, we have that

$$[\boldsymbol{J}(\boldsymbol{\eta})^{-1}]_{1:5,1:5} = \boldsymbol{J}(\boldsymbol{\eta}_{\mathrm{LOS}})^{-1}. \tag{15}$$

Hence, we can limit our discussion to the LOS path to be able to calculate the the PEB in (10). The partial derivatives needed in (12) can be expressed as

$$\frac{\partial\boldsymbol{\mu}_t}{\partial\rho_0} = e^{j\varphi_0}\boldsymbol{b}(\boldsymbol{p}_{\mathrm{ur}})^\top\boldsymbol{\omega}_t \,\boldsymbol{d}(\tau_0), \tag{16}$$

$$\frac{\partial\boldsymbol{\mu}_t}{\partial\varphi_0} = j\beta_0\boldsymbol{b}(\boldsymbol{p}_{\mathrm{ur}})^\top\boldsymbol{\omega}_t \,\boldsymbol{d}(\tau_0), \tag{17}$$

$$\frac{\partial\boldsymbol{\mu}_t}{\partial\boldsymbol{p}_{\mathrm{u}}} = \frac{2\beta_0\boldsymbol{b}(\boldsymbol{p}_{\mathrm{ur}})^\top\boldsymbol{\omega}_t}{c}\dot{\boldsymbol{d}}(\tau_0)\,\boldsymbol{u}_{\mathrm{ur}}^\top + \beta_0\boldsymbol{d}(\tau_0)\boldsymbol{\omega}_t^\top\dot{\boldsymbol{B}}(\boldsymbol{p}_{\mathrm{ur}}), \tag{18}$$

where we have used the following definitions:

$$\dot{\boldsymbol{d}}(\tau_0) \triangleq \frac{\partial\boldsymbol{d}(\tau_0)}{\partial\tau} = -j2\pi\Delta f \,\boldsymbol{n} \odot \boldsymbol{d}(\tau_0), \tag{19}$$

$$\dot{\boldsymbol{B}}(\boldsymbol{p}_{\mathrm{ur}}) \triangleq \frac{\partial\boldsymbol{b}(\boldsymbol{p}_{\mathrm{u}})}{\partial\boldsymbol{p}_{\mathrm{u}}} \tag{20}$$

$$= -j\frac{4\pi}{\lambda}\left(\mathrm{diag}\left(\boldsymbol{b}(\boldsymbol{p}_{\mathrm{ur}})\right)\boldsymbol{K}^\top - \boldsymbol{b}(\boldsymbol{p}_{\mathrm{ur}})\boldsymbol{u}_{\mathrm{ur}}^\top\right) \tag{21}$$

with $\boldsymbol{u}_{\mathrm{ur}} \triangleq \boldsymbol{p}_{\mathrm{ur}}/\|\boldsymbol{p}_{\mathrm{ur}}\|$, $\boldsymbol{K} \triangleq [\boldsymbol{u}_0, \boldsymbol{u}_1, \ldots, \boldsymbol{u}_{M-1}]$, $\boldsymbol{u}_m \triangleq (\boldsymbol{p}_{\mathrm{u}} - \boldsymbol{p}_{\mathrm{r},m})/\|\boldsymbol{p}_{\mathrm{u}} - \boldsymbol{p}_{\mathrm{r},m}\|$, and $\boldsymbol{n} \triangleq [0, 1, \ldots, N-1]$. Putting all of the above together, the FIM for the LOS path is

$$\boldsymbol{J}(\boldsymbol{\eta}_{\mathrm{LOS}}) = \frac{2E_{\mathrm{s}}}{\sigma_{\mathrm{n}}^2}\begin{bmatrix} NG & 0 & \Re\{\boldsymbol{z}^\top\} \\ 0 & N|\beta_0|^2 G & |\beta_0|\Im\{\boldsymbol{z}^\top\} \\ \Re\{\boldsymbol{z}\} & |\beta_0|\Im\{\boldsymbol{z}\} & \boldsymbol{H} \end{bmatrix}, \tag{22}$$

where we have used the definitions:

$$G \triangleq \sum_t |\boldsymbol{b}(\boldsymbol{p}_{\mathrm{ur}})^\top\boldsymbol{\omega}_t|^2, \tag{23}$$

$$\tag{24}$$

$$z^\top \triangleq \frac{2|\beta_0|}{c} G d^{\mathrm{H}} \dot{d} u_{\mathrm{ur}}^\top + N|\beta_0| b^H \mathbf{C}\dot{\mathbf{B}}, \tag{25}$$

$$H \triangleq \frac{4|\beta_0|^2}{c^2} G \|\dot{\mathbf{d}}\|^2 u_{\mathrm{ur}} u_{\mathrm{ur}}^\top$$
$$+ |\beta_0|^2 N \Re\left\{\dot{\mathbf{B}}^H \mathbf{C}\dot{\mathbf{B}}\right\} + \frac{2|\beta_0|^2}{c} \Re\left\{U + U^{\mathrm{H}}\right\}. \tag{26}$$

In the latter expressions, we have dropped the dependencies on τ_0 and p_{ur} for notation simplification. Furthermore, we used:

$$\mathbf{C} \triangleq \sum_t (\omega_t^* \omega_t^\top), \tag{27}$$

$$U \triangleq \left(\dot{\mathbf{d}}^H \mathbf{d}\right) u_{\mathrm{ur}} b^H \mathbf{C}\dot{\mathbf{B}}. \tag{28}$$

By using Schur's complement, we can calculate the equivalent FIM (EFIM) of p_u as

$$J(p_{\mathrm{u}}) = \frac{8|\beta_0|^2 E_{\mathrm{s}} G}{c^2 \sigma_{\mathrm{n}}^2} \left(\|\dot{d}\|^2 - \frac{|\dot{d}^{\mathrm{H}} d|^2}{N}\right) u_{\mathrm{ur}} u_{\mathrm{ur}}^\top \tag{29}$$
$$+ \frac{2 E_{\mathrm{s}}|\beta_0|^2 N}{\sigma_{\mathrm{n}}^2} \left(\Re\{\dot{\mathbf{B}}^{\mathrm{H}} F \dot{\mathbf{B}}\} - \frac{1}{G}\Re\{\dot{\mathbf{B}}^{\mathrm{H}} F b b^{\mathrm{H}} F \dot{\mathbf{B}}\}\right).$$

Then, the PEB in (10) can be computed as

$$\mathrm{PEB} = \sqrt{\mathrm{tr}\left(J(p_{\mathrm{u}})^{-1}\right)}. \tag{30}$$

Remark 2. *In far-field conditions, the vector $b(p_{\mathrm{ur}})$ can be approximated by b_{ff}, having the elements:*

$$[b_{\mathrm{ff}}(p_{\mathrm{ur}})]_m = \exp\left(\jmath \frac{4\pi}{\lambda} u_{\mathrm{ur}}^\top (p_{\mathrm{r},m} - p_{\mathrm{r}})\right). \tag{31}$$

In addition, the matrix $\dot{B}(p_{\mathrm{ur}})$ is approximated by

$$\dot{B}_{\mathrm{ff}}(p_{\mathrm{ur}}) = \frac{\partial b_{\mathrm{ff}}(p_{\mathrm{ur}})}{\partial p_{\mathrm{ur}}} \tag{32}$$
$$= \jmath \frac{4\pi}{\lambda\|p_{\mathrm{ur}}\|} \mathrm{diag}(b_{\mathrm{ff}}(p_{\mathrm{ur}})) M^\top \left(\mathbf{I} - u_{\mathrm{ur}} u_{\mathrm{ur}}^\top\right),$$

where the matrix M is given by

$$M = [p_{\mathrm{r},0} - p_{\mathrm{r}}, p_{\mathrm{r},1} - p_{\mathrm{r}}, \dots, p_{\mathrm{r},M-1} - p_{\mathrm{r}}], \tag{33}$$

and contains the relative positions of the RIS elements with respect to the surface's center. This implies that the EFIM in (29) consists of two components. The first one is proportional to $u_{\mathrm{ur}} u_{\mathrm{ur}}^\top$, and it is scaled by the signal bandwidth (due to the term $\|\dot{d}(\tau_0)\|$) and the energy reflected by the RIS towards the UE. The second component is proportional to $\mathbf{I} - u_{\mathrm{ur}} u_{\mathrm{ur}}^\top$, which means that it is in the two-dimensional subspace orthogonal to the first component. Moreover, this second component decreases with the UE distance as $1/\|p_{\mathrm{ur}}\|^2$ (without accounting here for any possible dependence of β_0 with the distance), and it is independent of the bandwidth. Note that the first component represents the contribution of the estimation of the propagation delay to the EFIM, while the second component corresponds to the contribution of the estimation of the direction of the UE (i.e., the angles of arrival and departure on/from the RIS). We next consider the case where the u_{ur} is orthogonal to the RIS normal n_{r}. Note that since $M^\top n_{\mathrm{r}} = 0$, we have that

$$M^\top \left(\mathbf{I} - u_{\mathrm{ur}} u_{\mathrm{ur}}^\top\right) = M^\top \left(\mathbf{I} - u_{\mathrm{ur}} u_{\mathrm{ur}}^\top - n_{\mathrm{r}} n_{\mathrm{r}}^\top\right). \tag{34}$$

Therefore, if $u_{\mathrm{ur}}^\top n_{\mathrm{r}} = 0$ holds, the term $\mathbf{I} - u_{\mathrm{ur}} u_{\mathrm{ur}}^\top - n_{\mathrm{r}} n_{\mathrm{r}}^\top$ becomes a one-dimensional subspace, which yields an ill-conditioned FIM.

V. LOW-COMPLEXITY LOCALIZATION

In this section, we present a low-complexity localization method for the considered RIS-aided wireless system. The proposed estimator has three steps: *i)* we first obtain a coarse estimate of the delay τ_0, then *ii)* we compute a coarse estimate of the relative UE position p_{ur}, and finally *iii)* we refine our estimation via maximizing the likelihood function.

A. Coarse Estimation of τ_0

The delay can be estimated by performing the inverse FFT (IFFT) of each vector $\tilde{y}_t$ and non-coherently accumulating the results. Specifically, we calculate the quantity:

$$y_{\mathrm{f}} \triangleq \sum_{t=1}^{T/2} \|F \tilde{y}_t\|^2, \tag{35}$$

where F is the $N' \times N$ IFFT matrix with elements $[F]_{r,s} = \exp\left(\jmath 2\pi rs/N'\right)/\sqrt{N'}$, where N' is a design parameter. Next, we estimate the delay as

$$\hat{\tau}_0 = \frac{1}{N'\Delta f} \arg\max_n |[y_{\mathrm{f}}]_n|. \tag{36}$$

B. Coarse Estimation of p_{ur}

Once the estimation $\hat{\tau}_0$ is available, we can generate the following sequence:

$$z \triangleq d(\hat{\tau}_0)^{\mathrm{H}} \left[\tilde{y}_1, \dots, \tilde{y}_{T/2}\right], \tag{37}$$

and formulate the cost function $P(p) \triangleq |s(p)z^{\mathrm{H}}|^2/\|s(p)\|^2$, where $s(p) = b(p)^\top \left[\tilde{\omega}_1, \tilde{\omega}_2, \dots, \tilde{\omega}_{T/2}\right]$. Using this cost function, we can estimate the UE position as $\hat{p}_{\mathrm{ur}} \triangleq \arg\max_p P(p)$. The evaluation of $P(p)$ is relatively simple since the vectors $s(p)$ can be precomputed on a grid of points, which can be stored at the RIS controller and made available to the UE. Moreover, $P(p)$ does not need to be evaluated in the full three-dimensional (3D) grid of points, but only in a 2D subgrid of points that fulfill $c\hat{\tau}_0/2 - \epsilon \leq \|p\| \leq c\hat{\tau}_0/2 + \epsilon$, where ϵ accounts for the range of errors in $\hat{\tau}_0$ and the density of the position grid.

C. Maximum Likelihood Position Estimation

We use the estimated $\hat{p}_{\mathrm{ur}}$ in Sec. V-B as a starting point to optimize the maximum likelihood (ML) function via a quasi-Newton algorithm. Based on (7), the ML estimator can be written as

$$\hat{p}_{\mathrm{ur}} \triangleq \arg\min_{p_{\mathrm{ur}}} \min_{\beta_0} \sum_{t=1}^{T/2} \|\beta_0 \zeta_t(p_{\mathrm{ur}}) - \tilde{y}_t\|^2 \tag{38}$$

$$= \arg\min_{p_{\mathrm{ur}}} \sum_{t=1}^{T/2} \|\beta_0(p_{\mathrm{ur}}) \zeta_t(p_{\mathrm{ur}}) - \tilde{y}_t\|^2, \tag{39}$$

where $\zeta_t(p_{\mathrm{ur}}) \triangleq d\left(2\|p_{\mathrm{ur}}\|/c\right) b(p_{\mathrm{ur}})^\top \tilde{\omega}_t$, and $\beta_0(p_{\mathrm{ur}}) \triangleq \sum_t \zeta_t(p_{\mathrm{ur}})^{\mathrm{H}} \tilde{y}_t/(\zeta_t(p_{\mathrm{ur}})^{\mathrm{H}} \zeta_t(p_{\mathrm{ur}}))$. Finally, the UE position can be estimated as $\hat{p}_{\mathrm{u}} = \hat{p}_{\mathrm{ur}} + p_{\mathrm{r}}$.

TABLE I
PARAMETERS USED IN THE SIMULATION RESULTS.

Parameter	Symbol	Value
Carrier frequency	f_c	28 GHz
Number of RIS elements	M	100×100
Light speed	c	3×10^8 m/s
RIS inter-element distance	d	$\lambda/4$
Number of subcarriers	N	3 000
Subcarrier bandwidth	ΔF	120 kHz
Number of transmissions	T	100
Transmit power	$N\Delta F E_s$	23 dBm
Noise power spectral density	N_0	-174 dBm/Hz
UE's noise figure	n_f	3 dB
Noise variance	$\sigma_n^2 \triangleq n_f N_0$	-171 dBm/Hz

VI. NUMERICAL RESULTS

In this section, we measure the accuracy of the proposed estimation method and calculate the PEBs for an example system whose parameters are listed in Table I, where N and ΔF are chosen based on the 5G NR numerology. Furthermore, we set $N' = 10N$. We assume that the RIS is located at the origin of the coordinate system with elements in the $z = 0$ plane. The channel gain is calculated as [21, Eq. (3)]

$$\beta_0 = \frac{\lambda^2 \cos(\phi)}{16\pi^{1.5}\|\boldsymbol{p}_{ur}\|^2},\qquad(40)$$

where $\phi = \cos^{-1}(\boldsymbol{u}_{ur}^\top \boldsymbol{n}_r)$ indicates the angle between the RIS normal ($\boldsymbol{n}_r$) and $\boldsymbol{p}_{ur}$. The distance between adjacent RIS elements was set to $d = \lambda/4$ based on Remark 1.

In Fig. 2 (a), we compare the positioning error of the proposed estimation method in Section V with the PEB in (10). The UE is located at $[d, d, d]/\sqrt{3}$ meters, where $d \in [1, 50]$. We consider the two RIS phase profile designs mentioned in Section III, specifically, the random and directional with $\delta = 1$ m. For each UE location the results are the average over 100 realizations of RIS phase profiles, for each of which 10 noise realizations were generated to calculate the positioning error. It can be seen that the proposed estimator can attain the theoretical lower bound for up to $d = 18$ m for the random phase design and $d = 29$ m for the directional one (with one exception point, which will be discussed later). With higher values of d, we can see from the PEBs that sub-meter UE localization is still possible, however, our low-complexity localization cannot achieve the bounds due to the low SNR.

In Fig. 2 (a), for directional profiles, there exists an exception point, which is at $d = 11$ m, where the estimation error is considerably higher than the PEB. This is due to the existence of one outlier. As mentioned in Section III-C, the directional codebook is generated by directing the beam towards random points inside the uncertainty area. If none of these points are in the close vicinity of the UE, then the received SNR is low and the estimator fails to localize. The probability of this event depends on the uncertainty area and the RIS beamwidth. Nonetheless, for the parameters considered in this paper, we can see that it is low. Figure 2 (b) shows the cumulative distribution function (CDF) for the PEB (solid lines) and estimation errors (dashed lines) for the point at

$d = 11$ m. It can be seen that the estimation error follows the PEB closely. Furthermore, it is shown that, due to the aforementioned outlier, the CDF of the estimation error for the directional profiles is saturated close to 1 (at 0.99).

In Fig. 2 (c), we illustrate the effects of the RIS size on the PEB at the UE location $\boldsymbol{p}_u = [10, 10, 10]/\sqrt{3}$. It can be seen that, for the directional phase profile, the PEB reduces with M faster than for the the random one. This is due to the fact that the SNR grows faster with M when directional beamforming is used. Furthermore, with very low values of M, different beams in directional codebook becomes almost identical (due to the very large beamwidths), which reduces the estimation accuracy. Hence, the directional codebook performs worse than the random one at (very) low values of M.

In Fig. 3 (a), we show the PEB for the UE position at $[x, y, y]$, where $x \in [-20, 20]$ and $y \in [0, 20]$. We consider one realization of random RIS phases. It can be seen that the PEB is almost symmetrical with respect to the y axis. Lower PEBs are obtained for lower values of θ, (partly) because of the RIS unit-cell directional pattern, which is incorporated in (40). As demonstrated, submeter localization is possible almost all across the considered area. In Fig. 3 (b), we study the PEB by setting β_0 to be the same for all the UE positions. They are set to the β_0 calculated at $[10, 10, 10]/\sqrt{3}$. By doing so, we can remove the effects of the SNR on PEB and focus on the geometrical effects. It can be seen that PEB increases with the UE distance and also θ; this behavior was explained in Remark 2.

VII. CONCLUSION

We presented the concept of 3D UE self-localization with only one RIS, where the UE transmits multiple OFDM signals and processes the reflected signal from the RIS. The positioning was performed by *i)* separating the signal reflected from the RIS from the undesired multipath, *ii)* establishing a coarse estimate of the position, and *iii)* refining the estimation via ML. We assessed the performance of the estimator in terms of the positioning error and compared it to an analytical lower bound. Our results provides a novel example where RISs become an enabling technology for radio localization. Note that, if in the proposed scenario, the RIS is replaced by a generic scatterer with a known location, then we could only estimate the distance $\|\boldsymbol{p}_{ur}\|$ (even in the absence of multipath). This of course would not be enough to find out the location of the UE. Future work includes the investigation of the effects of RIS impairments, NLOS components, and the UE mobility on the proposed system model and estimation approach.

REFERENCES

[1] C. Huang, A. Zappone, G. C. Alexandropoulos, M. Debbah, and C. Yuen, "Reconfigurable intelligent surfaces for energy efficiency in wireless communication," *IEEE Trans. Wireless Commun.*, vol. 18, no. 8, pp. 4157–4170, Aug. 2019.
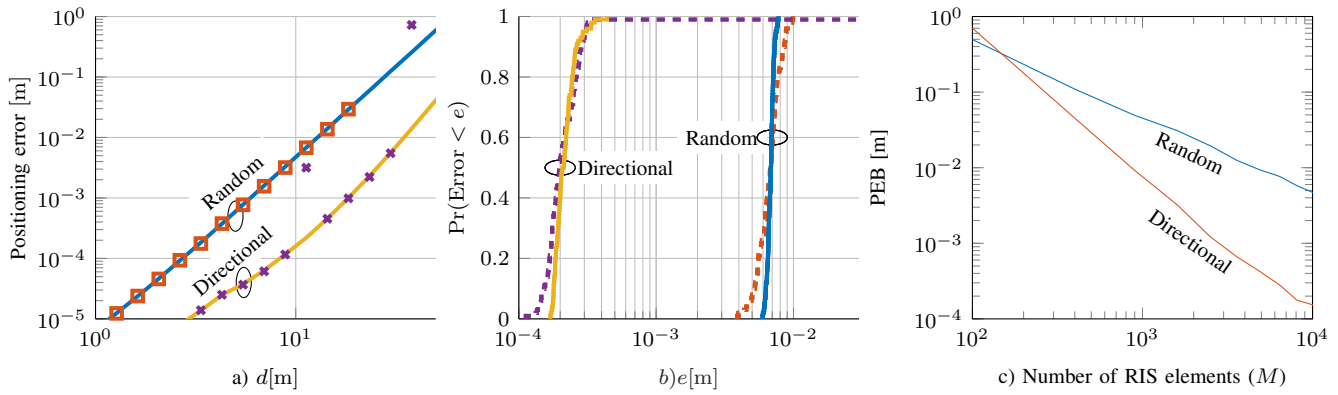
Fig. 2. Positioning errors for a system with a 100×100 RIS at the origin. (a) Estimation error (markers) and PEBs (solid lines) for a UE located at $\boldsymbol{p}_u = (d, d, d)/\sqrt{(3)}$, with random and directional RIS phase designs, (b) CDF of the estimation error (dashed lines) and PEB (solid lines) for $d = 11$m and 100 realizations of RIS phase profiles, (c) PEB at $\boldsymbol{p}_u = [10, 10, 10]/\sqrt{3}$ for different RIS sizes (M) and for directional and random codebooks.
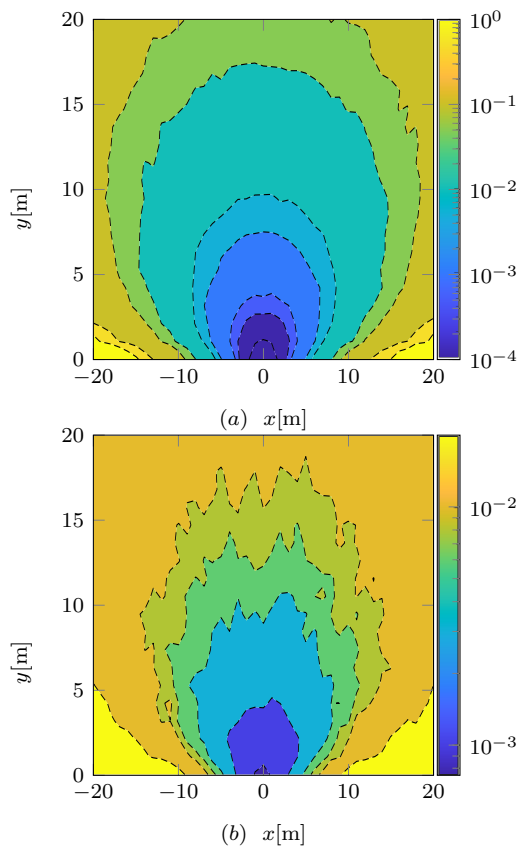

Fig. 3. Contour plot of the PEB in meters for the UE position $[x, y, y]$ for a random RIS phase profile, when the path loss is set a) according to (40), and b) equally for all the points (to the path loss at $[10, 10, 10]/\sqrt{(3)}$).

[2] Q. Wu and R. Zhang, "Towards smart and reconfigurable environment: Intelligent reflecting surface aided wireless network," *IEEE Commun. Mag.*, vol. 58, no. 1, pp. 106–112, Jan. 2020.

[3] G. C. Alexandropoulos, N. Shlezinger, and P. del Hougne, "Reconfigurable intelligent surfaces for rich scattering wireless communications: Recent experiments, challenges, and opportunities," *IEEE Commun. Mag.*, vol. 59, no. 6, pp. 28–34, Jun. 2021.

[4] E. Calvanese Strinati, G. C. Alexandropoulos, H. Wymeersch *et al.*, "Reconfigurable, intelligent, and sustainable wireless environments for 6G smart connectivity," *IEEE Commun. Mag.*, to appear, 2021.

[5] H. Wymeersch, J. He, B. Denis, A. Clemente, and M. Juntti, "Radio localization and mapping with reconfigurable intelligent surfaces: Challenges, opportunities, and research directions," *IEEE Veh.Technol. Mag.*, vol. 15, no. 4, pp. 52–61, Dec. 2020.

[6] D. Dardari, N. Decarli, A. Guerra, and F. Guidi, "Localization in NLOS conditions using large reconfigurable intelligent surfaces," in *Proc. IEEE SPAWC*, Sep. 2021.

[7] S. Hu, F. Rusek, and O. Edfors, "Beyond massive MIMO: The potential of positioning with large intelligent surfaces," *IEEE Trans. Signal Processing*, vol. 66, no. 7, pp. 1761–1774, Apr. 2018.

[8] Z. Abu-Shaban, K. Keykhosravi, M. F. Keskin, G. C. Alexandropoulos, G. Seco-Granados, and H. Wymeersch, "Near-field localization with a reconfigurable intelligent surface acting as lens," in *Proc. IEEE ICC*, Montreal, Canada, Jun. 2021.

[9] M. Rahal, B. Denis, K. Keykhosravi, B. Uguen, and H. Wymeersch, "RIS-enabled localization continuity under near-field conditions," in *Proc. IEEE SPAWC*, Jun. 2021.

[10] A. Fascista, A. Coluccia, H. Wymeersch, and G. Seco-Granados, "RIS-aided joint localization and synchronization with a single-antenna mmwave receiver," in *Proc. IEEE ICASSP*, Jun. 2021.

[11] K. Keykhosravi, M. F. Keskin, G. Seco-Granados, and H. Wymeersch, "SISO RIS-enabled joint 3D downlink localization and synchronization," in *Proc. IEEE ICC*, Montreal, Canada, Jun. 2021.

[12] K. Keykhosravi, M. F. Keskin, S. Dwivedi, G. Seco-Granados, and H. Wymeersch, "Semi-passive 3D positioning of multiple RIS-enabled users," *IEEE Trans. Vehicular Tech.*, to appear, 2021.

[13] H. Zhang, H. Zhang, B. Di, K. Bian, Z. Han, C. Xu, D. Zhang, and L. Song, "RSS fingerprinting based multi-user outdoor localization using reconfigurable intelligent surfaces," in *Proc. IEEE ISMICT*, Apr. 2021.

[14] A. Elzanaty, A. Guerra, F. Guidi, and M.-S. Alouini, "Reconfigurable intelligent surfaces for localization: Position and orientation error bounds," *IEEE Trans. Signal Process.*, vol. 69, pp. 5386–5402, Aug. 2021.

[15] Y. Liu *et al.*, "Reconfigurable intelligent surface aided wireless localization," in *Proc. IEEE ICC*, Montreal, Canada, Jun. 2021.

[16] S. Buzzi, E. Grossi, M. Lops, and L. Venturino, "Radar target detection aided by reconfigurable intelligent surfaces," *IEEE Signal Process. Lett.*, vol. 28, pp. 1315–1319, Jun. 2021.

[17] W. Lu, B. Deng, Q. Fang, X. Wen, and S. Peng, "Intelligent reflecting surface-enhanced target detection in MIMO radar," *IEEE Sensors Lett.*, vol. 5, no. 2, Feb. 2021.

[18] J. V. Alegría and F. Rusek, "Cramér-rao lower bounds for positioning with large intelligent surfaces using quantized amplitude and phase," in *Proc. Asilomar CSSC*, Pacific Grove, USA, Nov. 2019, pp. 10–14.

[19] K. Keykhosravi and H. Wymeersch, "Multi-RIS discrete-phase encoding for interpath-interference-free channel estimation," *[Online] https://arxiv.org/abs/2106.07065*, 2021.

[20] S. M. Kay, *Fundamentals of statistical signal processing: Estimation Theory*. Prentice Hall PTR, 1993.

[21] W. Tang, M. Z. Chen, X. Chen *et al.*, "Wireless communications with reconfigurable intelligent surface: Path loss modeling and experimental measurement," *IEEE Trans. Wireless Commun.*, vol. 20, no. 1, pp. 421–439, Jan. 2021.